Charge coupled devices for detection of coherent neutrino-nucleus scattering

Guillermo Fernandez Moroni,[1,2,3] Juan Estrada,[3] Eduardo E. Paolini,[2,4] Gustavo Cancelo,[3] Javier Tiffenberg,[3] and Jorge Molina[5]

[1]*Consejo Nacional de Investigaciones Científicas y Técnicas, C1033AAJ Buenos Aires, Argentina*
[2]*Universidad Nacional del Sur, Av. Alem 1253, 8000 Bahía Blanca, Argentina*
[3]*Fermi National Accelerator Laboratory, 60510 Batavia Illinois, USA*
[4]*Comisión de Investigaciones Científicas Provincia Buenos Aires, 1900 La Plata, Argentina*
[5]*Universidad Nacional de Asunción, 2160 Asunción, Paraguay*

(Received 11 September 2014; published 3 April 2015)

In this article the feasibility of using charge coupled devices (CCD) to detect low-energy neutrinos through their coherent scattering with nuclei is analyzed. The detection of neutrinos through this standard model process has been elusive because of the small energy deposited in such interaction. Typical particle detectors have thresholds of a few keV, and most of the energy deposition expected from coherent scattering is well below this level. The CCD detectors discussed in this paper can operate at a threshold of approximately 30 eV, making them ideal for observing this signal. On a CCD array of 500 g located next to a power nuclear reactor the number of coherent scattering events expected is about 3000 events/year. Our results shows that a detection with a confidence level of 99% can be reached within 16 days of continuous operation; with the current 52 g detector prototype this time lapse extends to five months.

DOI: 10.1103/PhysRevD.91.072001 PACS numbers: 13.15.+g

I. INTRODUCTION

Since the discovery of neutral-current neutrino interactions in 1973 by Hasert *et al.* [1], the importance of the coherent enhancement in elastic neutrino scattering has been pointed out [2], along with its implication for studies of star collapse. Unfortunately, it is difficult to detect because of its very small cross section ($<10^{-39}$ cm^2) [3] and the small energy deposition, typically less than 10 keV for any material. Detector technology has not met yet the extreme requirements on detector mass or on the energy threshold. Nevertheless, in recent times, interest for low energy neutrino physics has been increasing, mainly for verifying predictions of the standard model (SM), and exploring the possibilities of new physics beyond the SM at very small energy scales [4]. In astrophysics, for example, the understanding of MeV-neutrino physics has great relevance for energy transport in supernovas and it is related to the ongoing effort to develop new supernova detectors. These detectors can also be used to monitor nuclear reactors through their emitted neutrinos [5].

Although initially intended as memory devices [6,7], CCDs have found a niche as imaging detectors due to their ability to obtain high resolution digital images of objects placed in their line of sight. In particular, scientific CCDs have been used extensively in ground and space-based astronomy and X-ray imaging [8]. These devices have high detection efficiency, low noise, good spatial resolution and low dark current. Furthermore, thick CCDs with increased detection mass enable their use as particle detectors [9]. This technology is being used in the DAMIC experiment for cold dark matter search deployed at Snolab [10].

Several nuclear-reactor neutrino experiments were based mostly on inverse beta decay [11–13], usually using large volumes of target material to counter the relatively small cross section of this interaction. Recently, there has been a growing interest in using solid-state detectors for neutrino detection [14,15], taking advantage of the enhanced cross section by coherence.

In this paper, we analyze the feasibility of using CCD technology for neutrino scattering using a detector with a threshold of 28 eV of ionizing energy (five times larger than the RMS noise of 5.5 eV). It is expected that the low energy threshold of a CCD makes it possible to detect the main mechanism of neutrino-nucleus coherent scattering, which has never been observed. Our focus is on neutrinos with energies of less than 12 MeV produced at a nuclear reactor. The proposed detector uses a mass of up to 500 g of Si, which allows the construction of a small-sized nuclear-reactor neutrino detector.

II. HIGH RESISTIVITY SCIENTIFIC CCD

The cross section of a scientific CCD developed by Lawrence Berkeley National Laboratory and characterized extensively at Fermilab for the DECam project [9,16] is depicted in Fig. 1(a) showing the layout of the three gates that compose one pixel. The potential well generated under the gates in normal operation is represented in Fig. 1(b). CCDs with thickness of approximately 650 μm are available, and provide up to 5.2 grams of detector mass. Several million pixels CCD are fabricated on high resistivity silicon to maximize the depleted silicon volume, increasing their near-IR photon response. The CCD is fully depleted with the use of a substrate voltage. The array is divided into

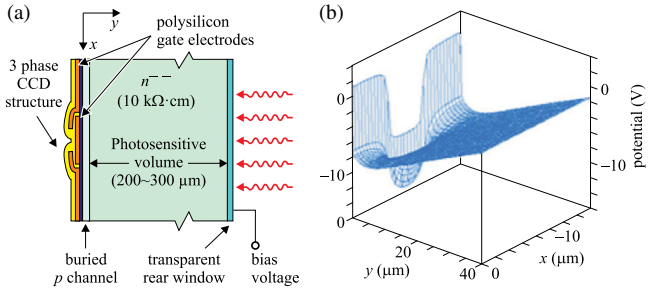

FIG. 1 (color online). Cross section of a 250 μm thick CCD developed at Lawrence Berkeley National Laboratory [17]. (a) Layout of the three gates that form one pixel. (b) Electrostatic potential (V) generated through the three gated phases shown as function of depth (y axis) and one of the lateral directions (x axis).

square pixels of 15 μm by 15 μm, providing enough spatial resolution for efficient rejection of some of the background particles.

A compendium of background events from measurements at sea level is shown in Fig. 2. Each particle produces a distinctive two-dimensional pattern in the CCD array. A muon is characterized by a straight-line track crossing the entire silicon volume. The small curved tracks are typical of energetic electrons produced by electromagnetic radiation. Alpha particles appear as big circular bright dots, due to the plasma effect they produce in the silicon [18]. Finally, point events formed by one or a few pixels, are produced by small depositions of energy by ionizing particles in one pixel volume. The coherent neutrino-nucleus scattering is expected to produce these kind of point events, as described in Sec. V B.

Besides the relatively large mass and high spatial resolution, an attractive feature of CCDs for neutrino detection is their very small energy threshold due to their good charge transfer efficiency, low readout noise and negligible dark-current contribution in a cooled system.

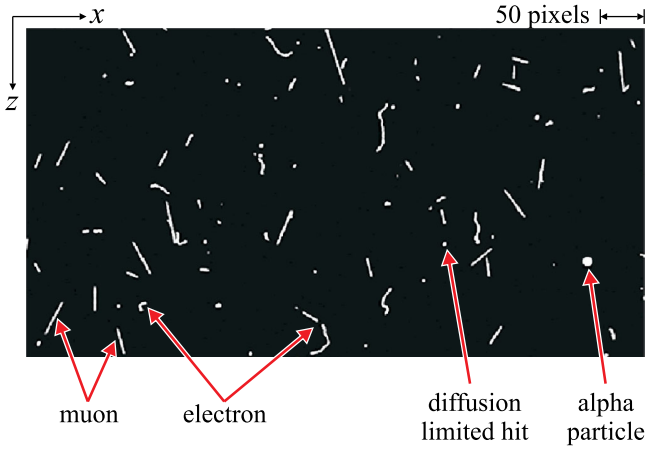

FIG. 2 (color online). Compendium of images from recent measurement of background at sea level in a CCD.

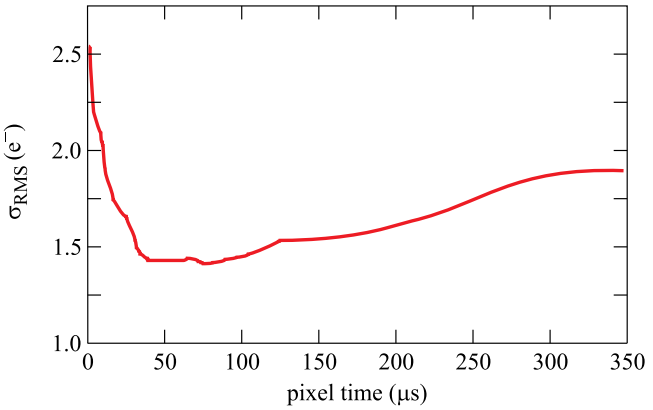

FIG. 3 (color online). RMS pixel error (σ_{RMS}) caused by the output amplifier, as a function of pixel read-out time.

The readout noise is added to each pixel by the output amplifier during the charge packet readout. It has a Gaussian distribution with a standard deviation (σ_{RMS}) that depends on the readout time of the pixel, as shown in Fig. 3 (see [19,20] for a detailed analysis). Because of the interaction between $1/f$ and white noise, an optimum readout noise with $\sigma_{RMS} = 1.5e^-$ (equivalent to 5.5 eV of ionization energy) can be achieved using a pixel readout time of 30 μs. In what follows, it is assumed that this noise level is achieved during normal operation of the detector. Figure 4 depicts a histogram of the values of individual pixels for this readout-time in the low energy region, when the CCD is exposed to a ^{60}Co source (blue solid curve), and with no source (red dashed curve). The peak near zero energy values represents the contribution of the output amplifier noise to empty pixels which determines the detection threshold of low energy depositions. The blue histogram also shows individual pixels with some charge which are part of events from energy depositions by the source.

Current fabrication techniques and materials have yielded CCD detectors with transfer inefficiencies below

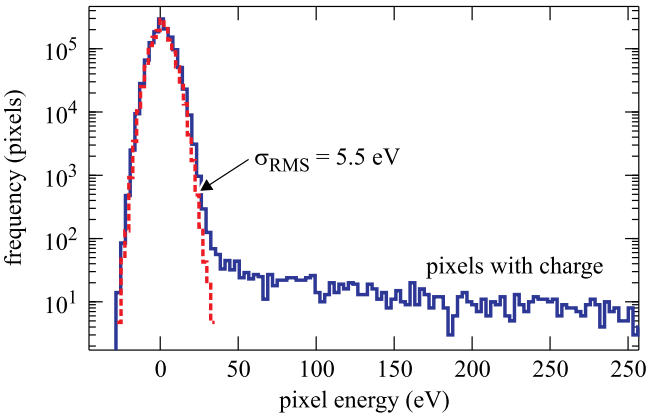

FIG. 4 (color online). Histogram of single pixels of images taken with a CCD running at 140 K and pixel-time of 30 μs.

15 ppm and dark-current generation below $2e^-$/day/pixel when cooled at 123 K, that have negligible effect on the detection of low energy particles.

III. NEUTRINO INTERACTION WITH MATTER

In the coherent neutrino-nucleus neutral-current interaction, a neutrino of any flavor scatters off a Si nucleus transferring some energy in the form of a nuclear recoil. The SM cross section σ for this process is [2,21]

$$\frac{d\sigma}{dE_{\bar{\nu}_e} dE_{rec}}(E_{\bar{\nu}_e}, E_{rec}) = \frac{G_F^2}{8\pi}[Z(4\sin^2\theta_W - 1) + N]^2 \times M\left(2 - \frac{E_{rec}M}{E_{\bar{\nu}_e}^2}\right)|f(q)|^2 \quad (1)$$

where M, N and Z are, respectively, the mass, neutron number and atomic number of the nucleus, $E_{\bar{\nu}_e}$ and E_{rec} are the incident neutrino and the nuclear recoil energy, G_F is the Fermi coupling constant, θ_W is the weak mixing angle, and $f(q)$ is the nuclear form factor at momentum transfer q. For $E_{\bar{\nu}_e} < 50$ MeV, where the momentum transfer (q^2) is small enough such that $q^2R^2 < 1$, where R is the radius of the nucleus [4], $|f(q)| \approx 1$, within an uncertainty of a few percent [22]. At small momentum transfers, the individual nucleon amplitudes are in phase and add coherently, so that the cross section increases by a factor of approximately N^2.

Although the cross section is enhanced by such coherence, elastic neutrino-nucleus scattering is difficult to observe because of the very small nuclear recoil energies. For silicon atoms the maximum event energy is $\max(E_{rec}) = 2E_{\bar{\nu}_e}^2/M$ (approximately 10 keV), showing that this measurement requires very sensitive detectors and a good characterization of the background.

The total cross section $\sigma_T(E_{\bar{\nu}_e})$ for a mono-energetic neutrino source of energy $E_{\bar{\nu}_e}$ is given by

$$\sigma_T(E_{\bar{\nu}_e}) = \frac{G_F^2}{4\pi}[Z(4\sin^2\theta_W - 1) + N]^2 E_{\bar{\nu}_e}^2$$

that can be approximated by

$$\sigma_T(E_{\bar{\nu}_e}) \approx 4.22 \times 10^{-45} N^2 E_{\bar{\nu}_e}^2 \quad (2)$$

when $E_{\bar{\nu}_e}$ is expressed in MeV and σ_T in cm^2. The total cross section σ_T for ^{28}Si ($N = 14$) is shown in blue trace in Fig. 5 as a function of the neutrino energy $E_{\bar{\nu}_e}$, showing the small probability for interaction of low energy neutrinos with matter, and its strong dependence on incident energy.

A nuclear power reactor is a high flux source of electron antineutrinos ($\bar{\nu}_e$) with energies up to 12 MeV, approximately. At such energies, the largest probability for interaction with Si atoms is given by the coherent neutrino-nucleus neutral-current interaction. The total cross section σ_T weighted by the $\bar{\nu}_e$ energy spectrum from a reactor ($dN_{\bar{\nu}_e}/dE_{\bar{\nu}_e}$) is also depicted in Fig. 5 using a red solid line, which is related to the probability of observing a reactor $\bar{\nu}_e$ of a given energy. The most probable event arises from neutrino energies between 2 and 4 MeV.

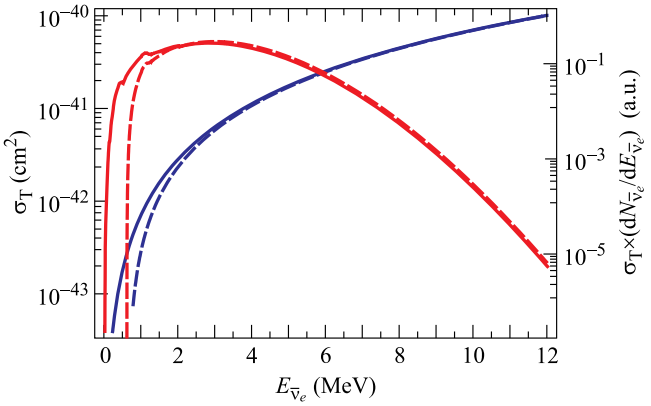

FIG. 5 (color online). Total neutrino-nucleus coherent cross section σ_T for silicon from Eq. (2) (blue curve, left), and weighted by the reactor antineutrino spectrum (red curve, right). The dashed curves correspond to a threshold energy of 28 eV, approximately $5\sigma_{RMS}$.

If the CCD threshold level is considered, the probability of detection is reduced, as depicted by the dashed curves in Fig. 5. In this case, the total cross section is calculated using a threshold of 28 eV, approximately 5 times the minimum RMS noise level (σ_{RMS}). These results, summarized in Fig. 5, suggest that the low threshold of the detectors is adequate for detecting $\bar{\nu}_e$ scattering.

IV. NEUTRINO SOURCE: NUCLEAR REACTOR

Nuclear reactors emit about 3.1×10^{16} $\bar{\nu}_e$/s per MW of thermal power, broadly distributed over energies up to 12 MeV, with a maximum between 0.5 MeV to 1 MeV. The antineutrinos come out isotropically from the core, so that the expected flux density at a distance L is diminished by the factor $1/(4\pi L^2)$. At steady state operation, approximately 7.3 $\bar{\nu}_e$ ($N_{\bar{\nu}_e}$) are produced per reactor fission [15].

Many processes are involved in antineutrino production, but the two major contributions are β decays of fission fragments of the four fissile isotopes ^{235}U, ^{238}U, ^{239}Pu, ^{241}Pu (≈6.1 $\bar{\nu}_e$/fission), and neutron capture by ^{238}U (≈1.2 $\bar{\nu}_e$/fission). The relative contribution from each source varies from reactor to reactor, as well as in a single reactor during a burning cycle, resulting in antineutrino flux scenarios that differ by a few percent. Although such variations are clearly noticeable, they are small enough to provide an essentially model-independent analysis of any reactor neutrino experiment.

In the following sections, each production mechanism is reviewed in more detail.

TABLE I. Relative fission contribution and neutrino yield per fission for the four fissile isotopes and the ^{238}U neutron capture. Typical values are given for integrated contributions.

Process	Relative rate for reactor fission	Neutrino yield ($N_{\bar{\nu}_e}$/process)	Neutrino yield ($N_{\bar{\nu}_e}$/fisision)
^{235}U	0.56	6.14	3.43
^{238}U	0.08	7.08	0.56
^{239}Pu	0.30	5.58	1.67
^{241}Pu	0.06	6.42	0.38
^{238}U(n,γ)	0.60	2.00	1.20

A. Antineutrinos from fissile isotopes

The $\bar{\nu}_e$ emitted in power reactors are predominantly produced through β-decays of the fission products, following the fission of the four dominant fissile isotopes: ^{235}U, ^{238}U, ^{239}Pu, and ^{241}Pu. Other fissile isotopes such as ^{236}U, ^{240}Pu, ^{242}Pu, etc., contribute less than 0.1% to the fissile isotope spectrum, and therefore can be neglected. Each isotope has a different $\bar{\nu}_e$ yield, $\bar{\nu}_e$ spectrum, and fission rate. Their content also changes during the fuel burning cycle, and leads to a small variation of the $\bar{\nu}_e$ flux and spectrum. This affects the total number $N_{\bar{\nu}_e}$ by a few percent, and can be ignored in a first order analysis of a CCD-based detector.

Typical $\bar{\nu}_e$ yield per element fission, as well as their relative contribution per reactor fission are summarized in Table I. The $\bar{\nu}_e$ spectrum produced through the fission of each isotope is depicted in Fig. 6 in units of $\bar{\nu}_e$/MeV for each process. These fluxes and spectra are provided in [15] for similar calculations on germanium detectors. The expected event analysis of Sec. V also considers new data of the antineutrino spectra between 2 and 8 MeV [23–25].

B. Antineutrinos from neutron capture in ^{238}U

The ^{238}U content in power reactors nuclear fuel varies between 95% to 97%. The ^{238}U nuclei absorb approximately

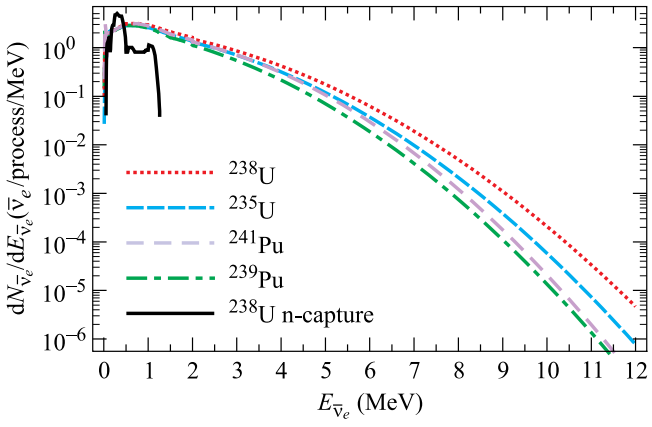

FIG. 6 (color online). Antineutrino spectrum for each process [15].

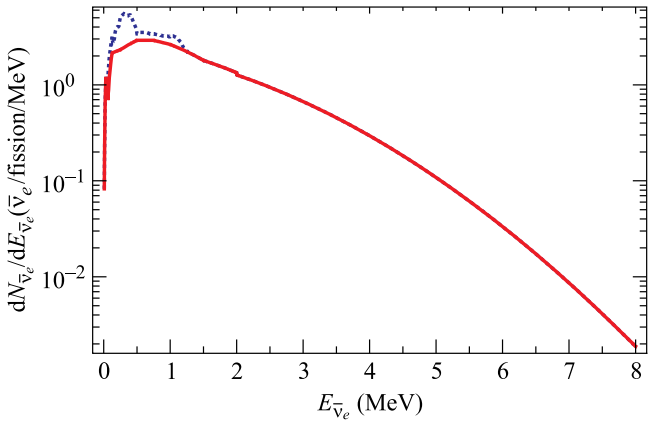

FIG. 7 (color online). Total reactor antineutrino spectrum per fission in the reactor per MeV. The red solid line reflects the fissile isotopes, and the blue dashed line the sum of the fissile isotopes and the neutron capture by ^{238}U.

0.6 neutrons per fission via the (n,γ) reaction: $^{238}\mathrm{U} + \mathrm{n} \Rightarrow {}^{239}\mathrm{U} \Rightarrow {}^{239}\mathrm{Np} \Rightarrow {}^{239}\mathrm{Pu}$. Two $\bar{\nu}_e$ are produced through β-decay of ^{239}U. This process contributes nearly 16% to the total $\bar{\nu}_e$ flux. The $\bar{\nu}_e$ yield and rate per fission at the reactor are also summarized in Table I. The energy of the antineutrinos produced by this process is below 1.3 MeV, as shown in Fig. 6 (black curve). A description of these processes can be found in [15].

Figure 7 depicts the total antineutrino spectrum per fission, obtained as weighted sum of the different contributions, with (blue dashed line) and without (red solid line) the contribution of the ^{238}U capture mechanism.

V. CCD EXPERIMENT AT REACTOR

This work provides a preliminary analysis to forecast the expectations for the Coherent Neutrino-Nucleus Interaction Experiment (CONNIE), currently under construction. The goal of CONNIE is the first unambiguous detection of neutrino-nucleus coherent scattering using an array of CCD detectors in a radiation shield located 30 meters from the core of the Angra II reactor, which operates at a thermal power of 3.95 GW. This experiment is being installed at the Almirante Alvaro Alberto Nuclear Central, in Angra Dos Reis, Brazil.

In steady-state operation, the neutrino flux produced by the reactor is 1.21×10^{20} $\bar{\nu}_e$/s approximately, and the flux density at the detector ($L = 30$ meters from the core) is 7.8×10^{12} $\bar{\nu}_e/\mathrm{cm}^2/\mathrm{s}$. Although these large numerical values suggest that nuclear power reactors may act as a neutrino source for the CONNIE experiment, the feasibility of neutrino detection requires not only the estimation of the event rates and background noise, but also the proper identification of neutrino events. Once these parameters are known, the running time of the experiment to achieve a certain confidence level can be estimated.

A. Event rate

The product of the coherent scattering interaction is a nuclear recoil that ionizes electrons of Si atoms in the lattice, which are collected to form the event in the output image. Using the differential cross section, the total $\bar{\nu_e}$ spectrum and the $\bar{\nu_e}$ flux expected at the detector, the nuclear recoil spectrum $\mathrm{d}R(E_{\mathrm{rec}})/\mathrm{d}E_{\mathrm{rec}}$ is given by

$$\frac{\mathrm{d}R}{\mathrm{d}E_{\mathrm{rec}}}(E_{\mathrm{rec}}) = N_t \int_{\sqrt{\frac{E_{\mathrm{rec}}M}{2}}}^{\infty} \mathrm{d}E_{\bar{\nu_e}} \frac{\mathrm{d}N_{\bar{\nu_e}}}{\mathrm{d}E_{\bar{\nu_e}}}(E_{\bar{\nu_e}}) \times \frac{\mathrm{d}\sigma}{\mathrm{d}E_{\bar{\nu_e}}\mathrm{d}E_{\mathrm{rec}}}(E_{\bar{\nu_e}}, E_{\mathrm{rec}}) \quad (3)$$

and the total rate for events R in the energy range of the detector is given by

$$R = \int_{E_{\mathrm{th}}}^{\infty} \mathrm{d}E_{\mathrm{rec}} \frac{\mathrm{d}R}{\mathrm{d}E_{\mathrm{rec}}}(E_{\mathrm{rec}}) \quad (4)$$

where $\mathrm{d}N_{\bar{\nu_e}}(E_{\bar{\nu_e}})/\mathrm{d}E_{\bar{\nu_e}}$ represents the spectrum of neutrinos at the detector, E_{th} is the detector's threshold energy, N_t is the number of nuclei in the detector, and $\sqrt{E_{\mathrm{rec}}M/2}$ is the minimum neutrino energy that can produce a recoil with energy E_{rec}.

The results for $\mathrm{d}R/\mathrm{d}E_{\mathrm{rec}}$ and R from Eqs. (3) and (4) are shown in Fig. 8 and Fig. 9, respectively. The nuclear recoil spectrum shown in Fig. 8 decreases rapidly with energy. Although events with E_{rec} up to 10 keV are expected, any recoil for $E_{\mathrm{rec}} > 3$ keV has a very low probability of occurrence. In fact, more than 96% of the events occur for $E_{\mathrm{rec}} < 2$ keV. This behavior can be also derived from the integrated spectrum in Fig. 9 (red curve), which represents the rate of events as a function of the upper limit in E_{rec}.

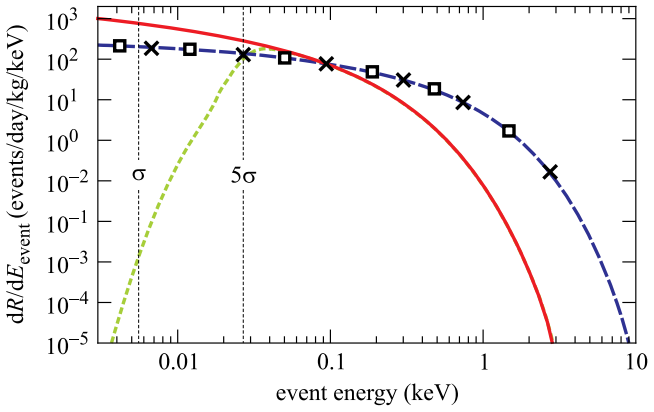

FIG. 8 (color online). Energy spectra for expected events in silicon detectors: (– – blue) nuclear-recoil energy spectrum, (— red) spectrum for detectable events using the quenching factor from Lindhard's theory and (- - - green) using the efficiency curve from detection algorithm in Sec. V C; recoil spectrum using neutrino calculations by Mueller *et al.* (□) [23] and Huber (×) [24].

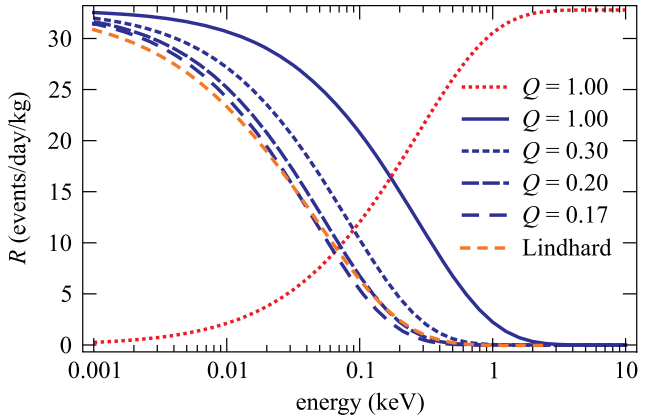

FIG. 9 (color online). Total number of events as a function of the threshold energy for different constant quenching factors (blue curves), and Lindhard factor (orange curve). The red dotted curve shows the total number of events as a function of the maximum detectable recoil energy using $Q = 1$.

Above 2 keV, the distribution becomes flat and there is essentially no significant increase in the event rate. This characteristic may be used to find the best energy cutoff to maximize the event to background ratio. The bounded energy range also provides some clues about the expected signature from $\bar{\nu_e}$-hits, as discussed in the next section. The use of heavier target materials result in an even shorter visible energy range.

Figure 8 also depicts the recoil spectrum using the reactor-antineutrino spectra of [23] and [24] with squares (□) and crosses (×), respectively, showing that the different models of the recoil spectrum are in good agreement for this energy range. Data used to derive these spectra include recent calculations of the ^{238}U antineutrino spectrum by Haag [25].

Only a fraction of the nuclear recoil energy is converted into charge inside the Si detector, because part of the deposited energy results in phonons, contributing to the increase of the thermal energy of the system. The quantity that reflects the mean ionization production by a nuclear recoil related to the ionization by an electron of the same energy is the quenching factor Q. This factor has a strong dependence on energy and unfortunately it is not well known for energies less than 4 keV, although the authors are involved in several ongoing efforts to measure Q within this energy range which include: fast neutron scattering on silicon target, electron capture decay by activated isotopes in CCD, and nuclear recoil energy calibration with a thermal neutron source. More details of these techniques can be found in [26]. However, measurements for event energies larger than 4 keV agree with Lindhard's theory [27,28]. Figure 10 shows the predicted silicon quenching factor by Lindhard, and a compendium of available measurements at different recoil energies [10]. Taking into account the Lindhard Q factor, the observable event energy spectrum is also shown as a solid curve in Fig. 8, indicating

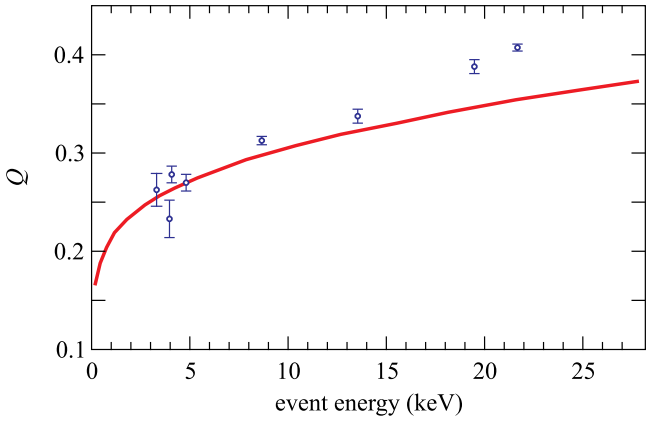

FIG. 10 (color online). Silicon quenching factor. Compendium of measurements of [10], and theoretical prediction by Lindhard [27,28].

that the range of ionization energy is reduced to approximately 3 keV. The dependence on lower ionizing energies becomes stronger due to the reduction of Q at small energy values.

Figure 9 also depicts the total number of detected events for different threshold energies and different quenching factor (Q) scenarios. Despite the fact that quenching factor is not well known at low energies, the total number of detected events has a relatively weak dependence on it because of the very low noise of CCD devices. Table II summarizes the number of events per kg per day of detector for the different factors and for two values of energy threshold E_{th}. The total number of events for zero energy threshold is expected to be 33 events per day per kg of silicon. If newer spectra models [23,24] are considered, data in Table II varies about 5%, which is a similar percentage to the variation expected from different burn-up conditions and reactor core compositions. Therefore, CCD detection capabilities are consistent for different available spectra models.

B. Identification of neutrino candidate events

The low energy nuclear recoil signature in the CCD corresponds to a diffusion limited hit, which means that the observed charge is generated in a volume smaller than the pixel size, and that the event is formed only by the diffusion of the free charge in the silicon [10].

When the charge is free to move in the Si lattice, the diffusion and drift mechanisms define its final lateral dispersion before it is trapped by the electric potential well under the gates. The lateral barriers extend approximately 10 μm in depth (y axes). Beyond this point, the electric field in the entire silicon bulk is uniform along the x and z axis, and varies only as a linear function of y (a detailed electrostatic description of the devices can be found in [9]). The net result is that most of the carriers reach the well of the gate in the same pixel in which they were generated, and only a small fraction transverse to adjacent pixels. Figure 11 depicts this lateral dispersion reconstructed from X-rays events. It shows the distribution of lateral standard deviation measured when the CCD is exposed to a ^{55}Fe source from the front (red curve) and from the back (blue curve). These profiles (continuous lines) closely resemble those obtained by simulation (dashed lines); minor differences appear because the simulation was tuned for another similar CCD. This experience suggest that the diffusion limited hit generated in the CCD volume can be modeled with a Gaussian distribution with a lateral deviation from 0 to 0.55 pixels.

The "pixelation" of the detector plays an important role in the final shape of the expected event, giving a 2D stepped representation of the Gaussian distribution expected from diffusion. Due to the small number of pixels composing the event, the shape of the stepped distribution depends strongly on the initial lateral position of the charge relative to the boundaries of the pixel. Figure 12 shows the effect of diffusion and pixelation on a simulated neutrino event produced at different depths and lateral positions. The energy of the event is 1.6 keV and it is simulated as interacting close to the gates of the CCD in the y axes (standard deviation of the diffusion distribution: $\sigma_{\mathrm{Diff}} = 0.2$ pixels) with a lateral position of $(x_i, z_i) = (2.1, 2.3)$ pixels in the array, in Fig. 12(a), and at $y \approx 250$ μm at the back of the detector ($\sigma_{\mathrm{Diff}} = 0.5$ pixels) with $(x_i, z_i) = (2.25, 1.6)$ in Fig. 12(b). A detailed description of the shape of diffusion limited hits can be found in [10,18,26,29,30].

TABLE II. Expected number of events for different quenching factors and threshold conditions, given in events/kg/day.

E_{th}	$Q = 1$	$Q = 0.3$	$Q = 0.2$	$Q = 0.17$	Lindhard
$1\sigma_{\mathrm{RMS}}$ (5.5 eV)	31.6	29.5	28.3	27.7	26.3
$5\sigma_{\mathrm{RMS}}$ (28 eV)	27.9	21.3	18.1	16.7	16.5

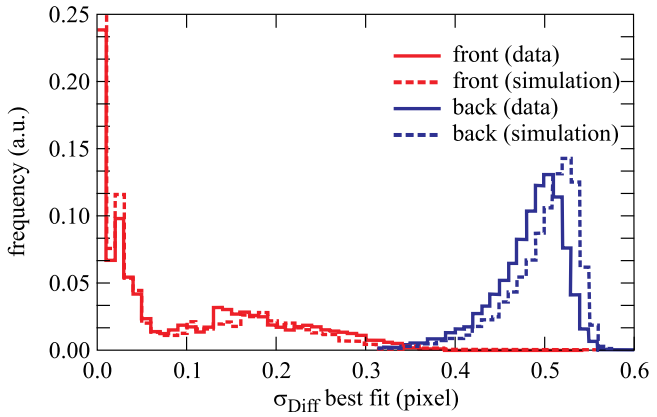

FIG. 11 (color online). Measurement and simulation of the reconstructed lateral deviation of events from X-rays from the K_α peak of a ^{55}Fe source when the CCD is exposed from the back (black curve) and from the front (red curve).

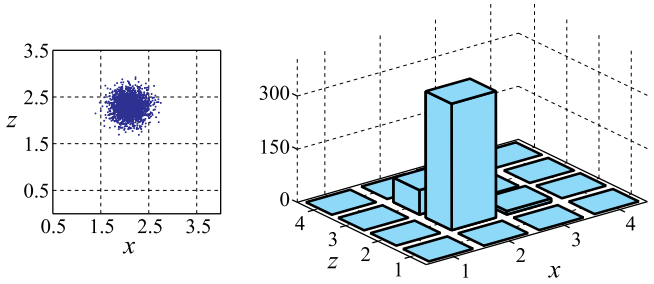

(a) $x_i = 2.10$, $z_i = 2.30$, $\sigma_{\mathrm{Diff}} = 0.2$ pixels

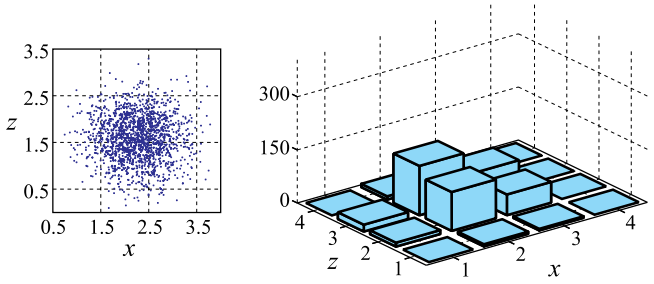

(b) $x_i = 2.25$, $z_i = 1.60$, $\sigma_{\mathrm{Diff}} = 0.5$ pixels

FIG. 12 (color online). Two simulated neutrino events generated at different depth of the detector and at different relative positions in the pixel. (a) $\bar{\nu}_e$-event interacting close to the gates of the detector, with $\sigma_{\mathrm{Diff}} = 0.2$ pixels, and (b) $\bar{\nu}_e$-event interacting close to the back (large y) of the detector, where $\sigma_{\mathrm{Diff}} = 0.5$ pixels. The x_i and z_i values are the coordinates of the point of origin of the events in the array.

The energy calibration of CCDs can be performed using several standard procedures. The most intuitive technique is using an X-ray source, specially ^{55}Fe. A full description of the procedure can be found in [8], and the calibration for these detectors in [10,26].

C. Detection efficiency

The detection efficiency strongly depends on the algorithm used to process the output images. Detection efficiency improves when the algorithm takes into account the charge distribution pattern discussed in the previous section, and when the signal to noise ratio is large.

We provide an estimation of the detection efficiency based on the signal to noise ratio, assuming that the use of the charge distribution patterns will enhance the discrimination between fake and meaningful events.

With CCD technology the signal to noise ratio can be enhanced by binning multiple pixels, i.e. summing the charges of neighborhood pixels to a single pixel. This is a typical procedure when reducing the size of the output image; see more details in [8]. Figure 13 shows the efficiency of a simple threshold detection algorithm of 28 eV when the CCD readout is configured for binning ten by ten pixels in boths dimensions. This curve can be used to obtain a more realistic scenario of the detectable neutrino

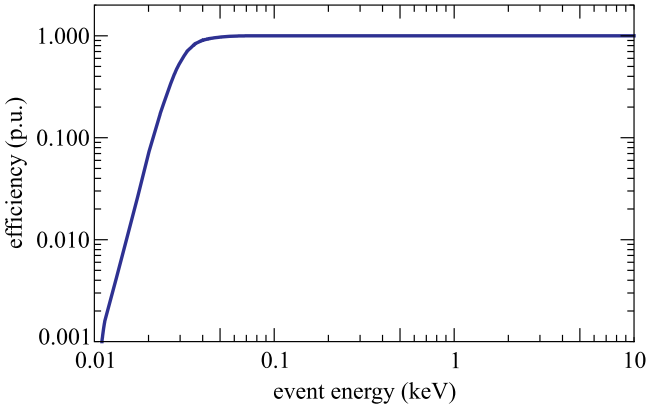

FIG. 13 (color online). Detection efficiency of a simple threshold algorithm of 28 eV when the CCD is configured for a binning of 10×10 pixels.

event spectrum and rate. The green dashed curve in Fig. 8 shows the effect of the detection efficiency on the detection of neutrino events below a few tens of eV. The detected rate is 16 events per day per kg of silicon, representing a reduction of 3% compared to the calculation using Lindhard predictions in Table II.

Refinements on the detection algorithm can improve the observable event rate. Efficient detection at low event energies can be improved using new techniques for CCD readout having a RMS readout noise below 3.65 eV [19,20]. Their implementations for this application is currently under development.

D. Running conditions and forecast

The current version of the CONNIE detector is based on 10 CCD running in parallel. The setup has capacity to read CCD of any thickness, with array sizes of up to 6 cm by 6 cm. The system was designed for easy on-site replacement of the detectors. The first stage of the experiment is considered a proof of concept of the technology, and uses ten 5.2 g CCD units. The final detector is expected to use a 500 g CCD-array.

The final spectrum and rate of events can be calculated from Figs. 8 and 9, respectively. The number of expected events considering the detector efficiency for several values of Q are summarized in Table III for both setups.

A rough estimation of the expected running time for the 52 g setup can be obtained considering the result as a counting experiment for a signal, expected to be higher than the Poisson fluctuation of the background at some given confidence level, for any specified energy range.

Figure 9 shows that for $Q < 0.3$ almost all the events have an ionization energy of less than 300 eV. For the energy range between 28 eV ($5\sigma_{\mathrm{RMS}}$) and 300 eV, and assuming Lindhard's factor and the efficiency in Fig. 13, the event rate from calculations in last subsection scaled down to 52 g is $0.84T$ events with T in days.

TABLE III. Expected number of events/day (events/year) in a CCD arrays of 52 g and 500 g assuming the detection efficiency from section V C and for different quenching factors.

Mass [g]	52	500
$Q = 1$	1.49 (524)	13.81 (5040)
$Q = 0.3$	1.09 (396)	10.43 (3809)
$Q = 0.2$	0.92 (336)	8.84 (3228)
$Q = 0.17$	0.85 (309)	8.15 (2975)
Lindhard	0.84 (305)	8.04 (2933)

TABLE IV. Expected running time for achieving different CL [PDG] for a detector's mass of 52 g and 500 g.

	T [days]	
CL [%]	52 g	500 g
80.00	012	11.2
90.00	028	12.9
95.00	045	14.7
98.00	070	17.3
99.87	150	15.8

Available bibliography shows that the count rate from background events in the low energy region at sea level using passive shield can be reduced to nearly 600 events/keV/day/kg [31], assuming that the material of the shield has a low level of radiative contamination. Similar rates of background have been reached using analogous configuration of CCD at shallow depth (30 m.w.e) in the Minos tunnel at Fermilab, and deep underground (600 m.w.e) at Snolab [10,26]. The background noise scaled by the mass of the detector and by the energy interval results in a rate of $8.5T$ events (T in days) for a 52 g detector.

Fake events due to the readout noise values above the energy threshold should be also considered. This rate depends on the number of pixel evaluations and the detection algorithm. Assuming 10 CCDs running in parallel being read every 2 hours and using a binning of ten by ten pixels, then the number of evaluations per day is 2.015×10^7. Considering a threshold of 28 eV, the rate of expected false positive events is $3.18T$ events with T in days.

A signal-to-noise ratio defined as

$$SNR = \frac{0.84T}{\sqrt{8.5T + 3.18T}} = 0.25\sqrt{T} \tag{5}$$

where T is the running time in days, can be used to obtain the corresponding confidence value. Therefore, the number of days running the experiment to achieve a certain confidence level (CL) can be computed, and some values for several CL values are listed in Table IV for a detector's mass of 52 and 500 g. These values were computed following the recommendations of [32].

VI. CONCLUSION

The capabilities of charge coupled devices to detect coherent neutrino-nucleus scattering interaction has been demonstrated. The low threshold achieved on these devices allows the detection of small energy depositions, in particular, nuclear recoils from neutrino scattering. On this energy range, the interaction is enhanced by coherence and therefore the neutrino signal can be observed using a system with moderate detecting mass.

The basis for a coherent neutrino nucleus scattering experiment at a nuclear reactor have been also reviewed, showing that a neutrino signal of more than 300 events per year can expected in a CCD array of 52 g, with a certainty greater than 99% over the background fluctuation after a hundred and fifty days of measurements.

ACKNOWLEDGMENTS

The authors wish to thank Dr. Tom Ferbel, University of Rochester, for his review of an early draft and his many suggestions, and the financial support from Fermi National Accelerator Laboratory, Consejo Nacional de Investigaciones Científicas y Técnicas, Universidad Nacional del Sur and Comisión de Investigaciones Científicas Provincia Buenos Aires.

[1] F. J. Hasert *et al.*, Phys. Lett. **46B**, 121 (1973).
[2] D. Z. Freedman, Phys. Rev. D **9**, 1389 (1974).
[3] D. Z. Freedman, D. N. Schramm, and D. L. Tubbs, Ann. Rev. Nucl. Part. Sci. **27**, 167 (1977).
[4] K. Scholberg, Phys. Rev. D **73**, 033005 (2006).
[5] E. Christensen, P. Huber, P. Jaffke, and T. E. Shea, Phys. Rev. Lett. **113**, 042503 (2014).
[6] W. S. Boyle, Rev. Mod. Phys. **82**, 2305 (2010).
[7] G. E. Smith, Rev. Mod. Phys. **82**, 2307 (2010).
[8] J. R. Janesick, *Scientific Charge Coupled Devices* (SPIE Publications, Bellingham, Washington, 2001).
[9] S. E.Holland, D. E. Groom, N. P. Palaio, F. J. Stover, and M. W., IEEE Trans. Electron Devices **50**, 225 (2003).
[10] J. Barreto *et al.*, Phys. Lett. B **711**, 264 (2012).
[11] Y. Abe *et al.* (Double Chooz Collaboration), Phys. Rev. Lett. **108**, 131801 (2012).

[12] J. K. Ahn *et al.* (RENO Collaboration), Phys. Rev. Lett. **108**, 191802 (2012).
[13] F. P. An *et al.* (Daya Bay Collaboration), Phys. Rev. Lett. **112**, 061801 (2014).
[14] B. Xin *et al.* (TEXONO Collaboration), Phys. Rev. D **72**, 012006 (2005).
[15] H. T. Wong *et al.* (TEXONO Collaboration), Phys. Rev. D **75**, 012001 (2007).
[16] J. Estrada *et al.*, Proc. SPIE Int. Soc. Opt. Eng. **6269**, 62693K (2006).
[17] H. Oluseyo, R. Meynart, S. P. Neeck, and H. Shimoda, Proc. SPIE Int. Soc. Opt. Eng. **5570**, 515 (2004).
[18] J. Estrada, J. Molina, J. J. Blostein, and G. Fernandez Moroni, Nucl. Instrum. Methods Phys. Res., Sec. A **665**, 90 (2011).
[19] G. I. Cancelo, J. C. Estrada, G. Fernandez Moroni, K. Treptow, T. Zmuda, and H. T. Diehl, Exp. Astron. **34**, 13 (2012).
[20] G. Fernandez Moroni, J. Estrada, G. Cancelo, S. E. Holland, E. E. Paolini, and H. T. Diehl, Exp. Astron. **34**, 43 (2012).
[21] K. Zuber, *Neutrino Physics* (CRC Press, Boca Raton, FL., 2011).
[22] K. Patton, J. Engel, G. C. McLaughlin, and N. Schunck, Phys. Rev. C **86**, 024612 (2012).
[23] Th. A. Mueller *et al.*, Phys. Rev. C **83**, 054615 (2011).
[24] P. Huber, Phys. Rev. C **85**, 029901 (2012).
[25] N. Haag, A Gutlein, M. Hofmann, L. Oberauer, W. Potzel, K. Schreckenbash, and F. M. Wagner, Phys. Rev. Lett. **112**, 122501 (2014).
[26] J. S. Tiffenberg *et al.*, in *Proceedings of the 33rd International Cosmic Ray Conference (ICRC2013), Rio de Janeiro, 2013*, edited by J. Knapp (Centro Brasileiro de Pesquisas Físicas, Rio de Janeiro, Brazil, 2013), p. 1243.
[27] J. Lindhard, V. Nielsen, M. Scharff, and P. V. Thomsen, Mat. Fys. Medd. K. Dan. Vidensk. Selsk **33**, 10 (1963).
[28] J. D. Lewin and P. F. Smith, Astropart. Phys. **6**, 87 (1996).
[29] A. Chavarria *et al.*, arXiv:1407.0347.
[30] G. Fernandez Moroni, E. E. Paolini, J. Estrada, and G. I. Cancelo, in *Proceeding of the Reunion de Trabajo en Procesamiento de la Informacion y Control (2013), Bariloche, 2013*, edited by J. Areta (Universidad Nacional de Río Negro, Argentina, 2013), p. 995.
[31] G. Heusser, Annu. Rev. Nucl. Part. Sci. **45**, 543 (1995).
[32] V. Buescher, J.-F. Grivaz, J. Hobbs, A. Kharchilava, G. Landsberg, J. Linnemann, H. Prosper, and S. Sldner-Rembold (Fermilab D0), Report No. Note-4629, 2004.